ELSEVIER

Journal of Power Sources 96 (2001) 352–368

JOURNAL OF POWER SOURCES

www.elsevier.com/locate/jpowsour

Design and part-load performance of a hybrid system based on a solid oxide fuel cell reactor and a micro gas turbine

P. Costamagna[a], L. Magistri[b], A.F. Massardo[b,*]

[a]*Dipartimento di Ingegneria Ambientale, Università degli Studi di Genova, Genova, Italy*
[b]*Dipartimento di Macchine, Sistemi Energetici e Trasporti, Università degli Studi di Genova, Genova, Italy*

Received 24 July 2000; accepted 7 November 2000

Abstract

This paper addresses the design and off-design analysis of a hybrid system (HS) based on the coupling of a recuperated micro gas turbine (MGT) with a high temperature solid oxide fuel cell (SOFC) reactor. The SOFC reactor model is presented and discussed, taking into account the influence of the reactor lay-out, the current density, the air utilisation factor, the cell operating temperature, etc. The SOFC design and off-design performance is presented and discussed; the design and off-design models of a recuperated micro-gas turbine are also presented. The operating line, the influence of the micro gas turbine ''variable speed'' control, and the efficiency behaviour at part load are analysed in depth.

Finally, the model of the hybrid system obtained by coupling the MGT and the SOFC reactor, considering the compatibility (technological constraints) of the two systems, is presented. The model allows the evaluation of the design and off-design behaviour of the hybrid system, particularly when the MGT variable speed control system is considered. The thermal efficiency of the hybrid system, taking into account its size (250/300 kW_e), is noteworthy: higher than 60% at design point, and also very high at part load conditions. Such a result is mainly due to the simultaneous positive influence of SOFC off-design behaviour and MGT variable speed control. Moreover, it is possible to recover the waste heat from the gas at the MGT recuperator outlet (T_{gas} is about 250°C) for cogeneration purposes.

1. Introduction

Solid oxide fuel cells (SOFCs) are electrochemical reactors currently under development for applications in the field of energy conversion [1,2]. The type of electrolyte which is usually employed (YSZ, yttria stabilised zirconia) requires a high operating temperature (1000°C) which imposes severe technological constraints on the materials, and thus several research programs are under way to find alternative electrolyte materials [3,4] or alternative multi-layer deposition techniques [5–7] which are expected to permit operation at temperatures of 700–800°C. Other intensive research efforts are being made in the field of electrode improvement, with particular attention to new electroactive materials and to the optimisation of the structure and morphology of composite electrodes [8,9]. As far as fuels are concerned, pure hydrogen and methane are currently being tested, and both internal and external steam reforming and partial oxidation reaction schemes have been proposed for the latter. Among the reactor geometries, planar [10] and tubular [11] reactor shapes have been proposed, with a number of variations such as planar cells with integrated air pre-heater [12]. Even though it is difficult to quote an average SOFC performance, the experimental data reported in the literature being distributed over a wide range, we can still state that, with an operating temperature in the range 900–1000°C, with pressure of 1 bar and hydrogen at the anode and oxygen at the cathode, the efficiency of the cell alone is at least 50%. SOFCs have not yet reached a level where they can compete with the cost, reliability and plant size reached by conventional energy conversion technologies; however, a number of demonstration programs are currently in progress, including some hybrid plants based on SOFCs coupled with small gas turbines [13,14].

Another power source, viewed as being well suited to meeting the needs of small energy users, is the small gas turbine. The first generation of micro-turbines [15–17] (25–300 kW_e), is currently being introduced into the distributed electrical power generation market. About a dozen companies are currently involved in the R&D of micro-turbines,

* Corresponding author. Tel.: +39-010-3532444; fax: +39-010-3532566.
E-mail address: massardo@unige.it (A.F. Massardo).

0378-7753/01/$ – see front matter
PII: S0378-7753(00)00668-6

Nomenclature

A, B	coefficients in Eq. (15) (ohm^{-1}, K)
C_1, C_2	coefficients in Eqs. (16) and (17) (ohm)
C_p	molar specific heat (J $kmol^{-1}$ K^{-1})
D_1, D_2	coefficients in Eqs. (18) and (19) (A)
E	activation energy (J $kmol^{-1}$)
F	molar flow rate (kmol s^{-1})
ΔG	Gibbs free energy change of reaction (J $kmol^{-1}$)
ΔG^0	standard Gibbs free energy change of reaction (J $kmol^{-1}$)
ΔH	enthalpy change of reaction (J $kmol^{-1}$)
I	electrical current (A)
$K_{p,\mathrm{ref}}$, $K_{p,\mathrm{shift}}$	equilibrium constants (Pa^2, –)
m_1, m_2	coefficients in Eqs. (13) and (14)
p	partial pressure (Pa)
p^0	reference pressure (Pa)
P	overall pressure (Pa)
R	reaction rate (mol s^{-1})
R_g	gas constant (J $kmol^{-1}$ K^{-1})
T	temperature (K)
U_o, U_f	oxygen, fuel utilisation factor
V_{oc}	thermodynamic electrical potential (V)
V_p	loss of electrical potential (V)
V	electrical potential of stack (V)
W_{el}	electrical power (W)
x	molar fraction
Greek letters	
Ω	electrical resistance (ohm)
v	stoichiometric coefficient
ρ	electrical resistivity (ohm cm)
Subscripts	
a, c, el	anode, cathode, electrolyte
con	contact
i	chemical component
j	flow stream
k	chemical (or electrochemical) reaction
ohm	ohmic
pol	polarisation
Superscripts	
in, out	inlet, outlet

and several of these projects have been discussed previously [18]. To meet low-cost goals the engine configurations are kept as simple as possible, with many of the machines embodying the following features: (1) single-stage radial compressor; (2) single-stage radial inflow turbine: (3) direct-drive high-speed air-cooled generator; (4) multi-fuel combustor; (5) highly effective compact recuperator; and (6) a simple control system. An additional attractive feature is the use of air bearings to support the single high-speed rotor. The salient features of a representative micro-turbine are given by Massardo et al. [15], Mc Donald [16], and Rodgers [17]. With a compressor pressure ratio of about 4, a turbine inlet temperature of 880–900°C, and a recuperator effectiveness of 0.85–0.88, the estimated thermal efficiency is about 30% ($50 \div 100\ kW_e$). Factoring in other aspects, including the generator and the power required for the fuel compressor, the overall efficiency of the microturbine that stands alone is about 27%. To advance significantly beyond this level will require an increase in turbine inlet temperature, which will necessitate the use of ceramics in the hot-end components [15].

Solid oxide fuel cells (SOFCs) integrated with gas turbines of small size (less than 1 MW) are attracting wide interest [19–24] as these systems are able to simultaneously solve some of the key problems of small gas turbines (low efficiency and NO_x emissions due to the combustor) and of SOFCs (high cost, predicted to be around $1000–1500 per kW). The pressurised SOFC module substitutes the combustor of the regenerated turbine plant, and the clean effluent has a temperature of about 900°C, which well matches the requirements on the inlet temperature of first generation micro-turbines. The value of the compressor discharge pressure of about 4 bar also facilitates increased power output and higher efficiency from a given SOFC frame size [19]. Plant efficiencies are predicted to be close to 60%, and thus the cost of the resulting energy should be lower than that of a gas turbine plant of the same size (taking into account both capital and variable costs). Integrated SOFC/microturbines (hybrid systems) are at an early stage of testing at the moment [19], and technical-economic optimisation is an issue currently being addressed by many developers.

In this paper, the design and off-design performance of a small size power hybrid system (HS) obtained by coupling a micro gas turbine ($50\ kW_e$) and a SOFC tubular reactor is discussed on the basis of a model of the hybrid system, obtained by coupling the design — off-design models of the micro gas turbine and the tubular SOFC reactor, respectively. All the models, written in the Matlab language, are presented and discussed in detail in this paper. Then, the design and part load performance of the MGT, SOFC reactor, and HS are presented and discussed in depth, also taking into account the influence of the MGT variable speed control system. The details of the configuration of the SOFC module, GT group and overall plant are discussed and presented together with the modelling equations in the next section of the paper.

2. Configuration and model of the MGT–SOFC hybrid plant

2.1. SOFC group

Fig. 1 shows the lay-out of the SOFC group, which includes both the reformer and the SOFC stack. The refor-

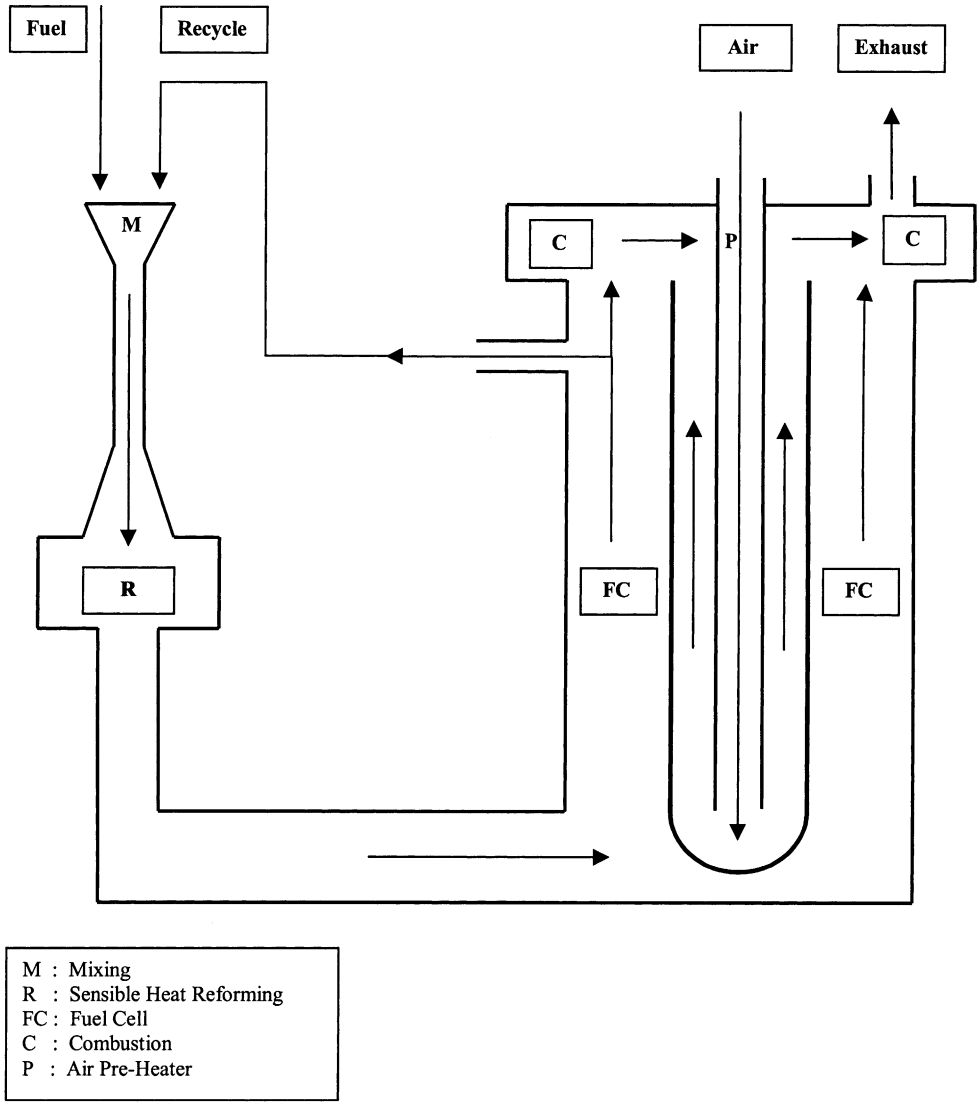

Fig. 1. Scheme of the SOFC group, including the SOFC stack, the mixer and the sensible heat reformer.

mer is a typical catalytic reactor, where the following reactions take place:

$$CH_4 + H_2O \leftrightarrow CO + 3H_2 \text{ (reforming)} \quad (1)$$

$$CO + H_2O \leftrightarrow CO_2 + H_2 \text{ (shifting)} \quad (2)$$

The sensible heat of the reactants provides the energy necessary for the reforming reaction to occur. The reactants are methane and water, which are supplied to the reformer through the fuel and the recycling of the water-rich anodic-exhaust of the SOFC; the composition of the anodic recycle under typical operating conditions (design point) is $x_{H_2O} = 0.4430$; $x_{H_2} = 0.00405$; $x_{CO} = 0.04088$; $x_{CO_2} = 0.5120$. In this study, the recycled flow rate is chosen in order to meet the condition that the steam-to-carbon ratio be about 2.4; this condition ensures that the problem of carbon deposition is avoided in the SOFC stack. The other components of the SOFC group are the mixer and the SOFC stack. The mixer is an ejector, where the fuel and the recycled flow rate mix prior to entering the reformer. The SOFC group is represented in Fig. 1 as a bundle of tubular cells; however, no specific details of the tubular geometry have been taken into consideration in the simulation. After the recycled flow rate has been drawn from the anodic side, the SOFC exhausts mix and burn in the outlet part of the SOFC stack so that their temperature rises to the level required by the downstream MGT group.

In this study, the SOFC simulation is a sub-module of the overall plant model, which requires many iterations before reaching convergence; owing to this fact, reliability and high calculation speed are the most important requirements for the SOFC subroutine. In order to meet these requirements, some authors [25] have proposed a predictive evaluation of the behaviour of the SOFC group based on the interpolation of experimental data of reactor behaviour under different operating conditions. However, due to the high number of operating variables (temperature, current density, reactant

utilisation, pressure, etc.), a complete experimental database of SOFC performance under the different operating conditions is difficult to obtain, and no data are available in the open literature yet. Moreover, as SOFC reactors are still under development, a 'state of the art' fuel cell performance cannot be defined, and it would be very useful to have a flexible simulation tool, which could easily be adapted to different cell geometries and operating conditions, but this is only possible with a model based on mass and energy balances coupled with appropriate expressions for the reaction kinetics, thermodynamic constants and material properties. Thus, such a model has been developed in order to evaluate the behaviour of the SOFC group, including mixer, reformer and SOFC stack. The modelling approach followed in this study is somewhat different from the one adopted in previous works [26,27], where the balance equations were written as local balances, under the form of partial differential equations. Those equations were then integrated numerically along the SOFC geometrical coordinates, allowing a detailed evaluation of the distribution of the physical–chemical variables (temperature, gas compositions, electrical current density, etc.) within the SOFC. Instead, in this study, the balance equations are written as macroscopic balances, in the form of finite equations. Those equations simply express a balance between inlet and outlet flows of mass and energy in each component of the group; under suitable assumptions (reported and discussed below), those equations allow the evaluation of the average values of the physical–chemical variables (i.e. temperatures, concentrations, etc.) of each component, and the electrochemical performance of the group itself. Obviously, this approach is greatly simplified and less accurate than the previous one; this loss of accuracy is fully acceptable within the framework of the overall plant evaluation and allows a significant reduction in the computational time.

The following assumptions have been made: (1) adiabaticity of all the components of the SOFC group; (2) uniformity of temperature within all the components of the SOFC group; (3) cathodic flow composed of O_2 and N_2; (4) anodic flow composed of CH_4, CO, CO_2, H_2, H_2O; (5) reforming and shift reactions at equilibrium in the reformer and the SOFC stack; (6) electrochemical reactions in the SOFC stack as reported below:

$$\begin{aligned} &\tfrac{1}{2}O_2 + 2e^- \rightarrow O^{2-} \quad \text{cathode} \\ &H_2 + O^{2-} \rightarrow H_2O + 2e^- \quad \text{anode} \\ &H_2 + \tfrac{1}{2}O_2 \rightarrow H_2O \quad \text{overall reaction} \end{aligned} \tag{3}$$

the electrochemical oxidation of CO has not been taken into account at this stage; (7) temperatures of the gases at the outlet of the reformer and the SOFC stack are equal to the reformer and stack temperatures, respectively; some results previously published in the literature [26,28,29] support this hypothesis.

The equations used for the simulation of the various elements of the SOFC group are reported in Table 1. The equations of the mixer simply express the conservation of mass and energy through the mixing process. The equations of mass and energy balance for the reformer (Eqs. (8) and (9)) include, in addition to the input and output contributions, the generation term due to the chemical reactions. The reaction rates R_k (where $k = 1$ for the reforming reaction, and $k = 2$ for the shift reaction) are evaluated through Eqs. (6) and (7), which express an equilibrium condition. The assumption of thermodynamic equilibrium, at an operating temperature which is about 550°C (see Section 3.2) is fully justified in the presence of a suitable catalyst in the reforming reactor. For the sake of completeness, the partial pressures of the reactants in Eqs. (6) and (7) are related to the molar flow rates F through the relationship

$$p_i = \frac{F_i}{F} P \tag{24}$$

In the SOFC stack, the calculation of the electrical current–voltage relationship is made through the evaluation of the thermodynamic voltage (Eq. (12)), which is the voltage of the stack under open-circuit conditions. When electrical current is drawn from the stack, voltage losses arise due to irreversibilities. These losses can be classified as: (1) ohmic losses (Eqs. (13)–(15)); (2) activation losses, due to sluggish electrode kinetics (Eqs. (16) and (17)); (3) concentration losses, occurring when the diffusion of the reactants through the electrodes is slower than the electrochemical reaction. However, at the high operating temperature of SOFCs, diffusion is a very efficient process, and thus the latter effect is usually negligible, unless under conditions of very high fuel or oxidant utilisation, which are not taken into consideration here. Thus, concentration losses have been neglected in this work. The current–voltage behaviour of the stack is evaluated by subtracting the overall voltage losses from the thermodynamic potential (Eqs. (21) and (22)) for each value of the electrical current.

The balance equations of the SOFC stack account for the process of conversion of chemical energy to electrical energy. Thus, in the mass balance (Eq. (22)) both chemical end electrochemical reactions have been included, and the k index varies between 1 and 3, where $k = 1$ for the reforming, $k = 2$ for the shift reaction and $k = 3$ for the electrochemical reaction. In this case, the shift and reforming reaction rates are also evaluated from the constant of thermodynamic equilibrium (Eqs. (10) and (11)); the electrokinetics R_3 is correlated to the electrical current I supplied by the stack

$$R_3 = \frac{I}{2F} \tag{25}$$

The energy balance (Eq. (23)) includes the electrical power W_{el} and the enthalpy changes of the chemical and electrochemical reactions, and allows the evaluation of the

Table 1
Basic equations for the simulation of the SOFC group

Mixer	Mass balance	$F_i^{\text{out}} = \sum_j F_{i,j}^{\text{in}}$	(4)
	Energy balance	$T^{\text{out}} = \frac{\sum_i C_{p,i} \sum_j F_{i,j} T_j^{\text{in}}}{\sum_i F_i^{\text{out}} C_{p,i}}$	(5)
Reformer	Equilibrium chemical reactions	$K_{p,\text{ref}} = \frac{p_{\text{H}_2}^3 p_{\text{CO}}}{p_{\text{CH}_4} p_{\text{H}_2\text{O}}}$ (reforming)	(6)
		$K_{p,\text{shift}} = \frac{p_{\text{CO}_2} p_{\text{H}_2}}{p_{\text{CO}} p_{\text{H}_2\text{O}}}$ (shifting)	(7)
	Mass balance	$F_i^{\text{out}} = F_i^{\text{in}} + \sum_k \nu_{i,k} R_k$	(8)
	Energy balance	$T^{\text{out}} = \frac{\sum_i F_i^{\text{in}} C_{p,i} T^{\text{in}} + \sum_k R_k (-\Delta H_k)}{\sum_i F_i^{\text{out}} C_{p,i}}$	(9)
Fuel cell stack	Equilibrium chemical reactions	$K_{p,\text{ref}} = \frac{p_{\text{H}_2}^3 p_{\text{CO}}}{p_{\text{CH}_4} p_{\text{H}_2\text{O}}}$ (reforming)	(10)
		$K_{p,\text{shift}} = \frac{p_{\text{CO}_2} p_{\text{H}_2}}{p_{\text{CO}} p_{\text{H}_2\text{O}}}$ (shifting)	(11)
	Electrochemical reaction	$V_{\text{oc}} = \frac{-\Delta G}{2F} = \frac{-\Delta G^0}{2F} + \frac{R_{\text{g}} T}{2F} \ln \frac{p_{\text{H}_2} (p_{\text{O}_2})^{1/2}}{p_{\text{H}_2\text{O}}}$	(12)
		$\rho_{\text{el}} = A_{\text{el}} \exp\left(-\frac{B_{\text{el}}}{T}\right)$	(13)
		$\rho_{\text{a}} = A_{\text{a}} \exp\left(-\frac{B_{\text{a}}}{T}\right)$	(14)
		$\rho_{\text{c}} = A_{\text{c}} \exp\left(-\frac{B_{\text{c}}}{T}\right)$	(15)
		$\frac{1}{\Omega_{\text{pol,a}}} = D_1 \frac{2F}{R_{\text{g}} T} \left(\frac{p_{\text{H}_2}}{p^0}\right)^{m_1} \text{e}^{-(E_{\text{a}}/RT)}$	(16)
		$\frac{1}{\Omega_{\text{pol,c}}} = D_2 \frac{4F}{R_{\text{g}} T} \left(\frac{p_{\text{O}_2}}{p^0}\right)^{m_2} \text{e}^{-(E_{\text{c}}/RT)}$	(17)
		$\Omega_{\text{tot}} = \sum \Omega_{\text{ohm}} + \sum \Omega_{\text{pol}} + \Omega_{\text{con}}$	(18)
		$V_p = \Omega_{\text{tot}} I$	(19)
		$V = V_{\text{oc}} - V_p$	(20)
		$W_{\text{el}} = VI$	(21)
	Mass balance	$F_i^{\text{out}} = F_i^{\text{in}} + \sum_k \nu_{i,k} R_k$	(22)
	Energy balance	$T^{\text{out}} = \frac{\sum_i F_i^{\text{in}} C_{p,i} T^{\text{in}} + \sum_k R_k (-\Delta H_k) - W_{\text{el}}}{\sum_i F_i^{\text{out}} C_{p,i}}$	(23)

outlet temperature of the gases, which is equal to the average temperature of the stack. As the latter temperature is an input value for the calculation of the stack current–voltage relationship (as T appears in Eqs. (12)–(17) discussed above), the system of Eqs. (4)–(25) was solved through a numerical method, starting from a first-attempt value for the stack temperature and calculating a new temperature at each iteration until convergence was reached.

The values of all the parameters appearing in Eqs. (13)–(19) have been taken from the literature [27,30,31] and are reported in Table 2.

2.2. Micro gas turbine

Fig. 2 shows a simplified lay out of a recuperated micro gas turbine. The MGT is made of the following components:

Table 2
Values of the parameters appearing in the equations reported in Table 1

Coefficient in Eq. (13)	$A_{el} = 0.00294$ (Ω cm)
Coefficient in Eq. (13)	$B_{el} = -10350$ (K)
Coefficient in Eq. (14)	$A_a = 0.00298$ (Ω cm)
Coefficient in Eq. (14)	$B_a = 1392$ (K)
Coefficient in Eq. (15)	$A_c = 0.008114$ (Ω cm)
Coefficient in Eq. (15)	$B_c = -600$ (K)
Coefficient in Eq. (16)	$D_1 = 2.13 \times 10^4$(A/cm^2)
Coefficient in Eq. (17)	$D_2 = 1.49 \times 10^4$(A/cm^2)
Anodic activation energy	$E_a = 110000$ (J Kmol^{-1})
Catodic activation energy	$E_c = 110000$ (J Kmol^{-1})
Contact resistance	$\Omega_{con} = 0.15$ (Ω)
Cathode thickness	0.035 (cm)
Electrolyte thickness	0.017 (cm)
Anode thickness	0.030 (cm)

centrifugal compressor, inflow expander, combustion chamber, recuperator, electrical generator, natural gas compressor.The simulation program is composed of several modules representing actual interconnected MGT components [32].

The simulation of the compressor module is based on the experimental maps (efficiency and pressure ratio versus non-dimensional flow rate) shown in Fig. 3 [33]. The calculation is checked at every step to make sure the compressor surge margin is respected. The input data of the compressor module are: air inlet pressure and temperature, rotational speed, and a first guess pressure ratio. The actual pressure ratio value of MGT is determined using a matching technique between the compressor and the downstream components [34].

In the combustion chamber the complete combustion reaction hypothesis is utilised, using the outlet compressor data and the fuel mass flow rate as input. The combustion chamber pressure losses (correlated to the combustion process and to the friction) are evaluated in the program [34].

The simulation of the expander is based on the turbine non-dimensional maps shown in Fig. 4 [35], and utilises the data at the combustion chamber outlet and the regenerator downstream pressure losses as inputs. The mass flow rate and compressor-turbine work compatibility are checked to

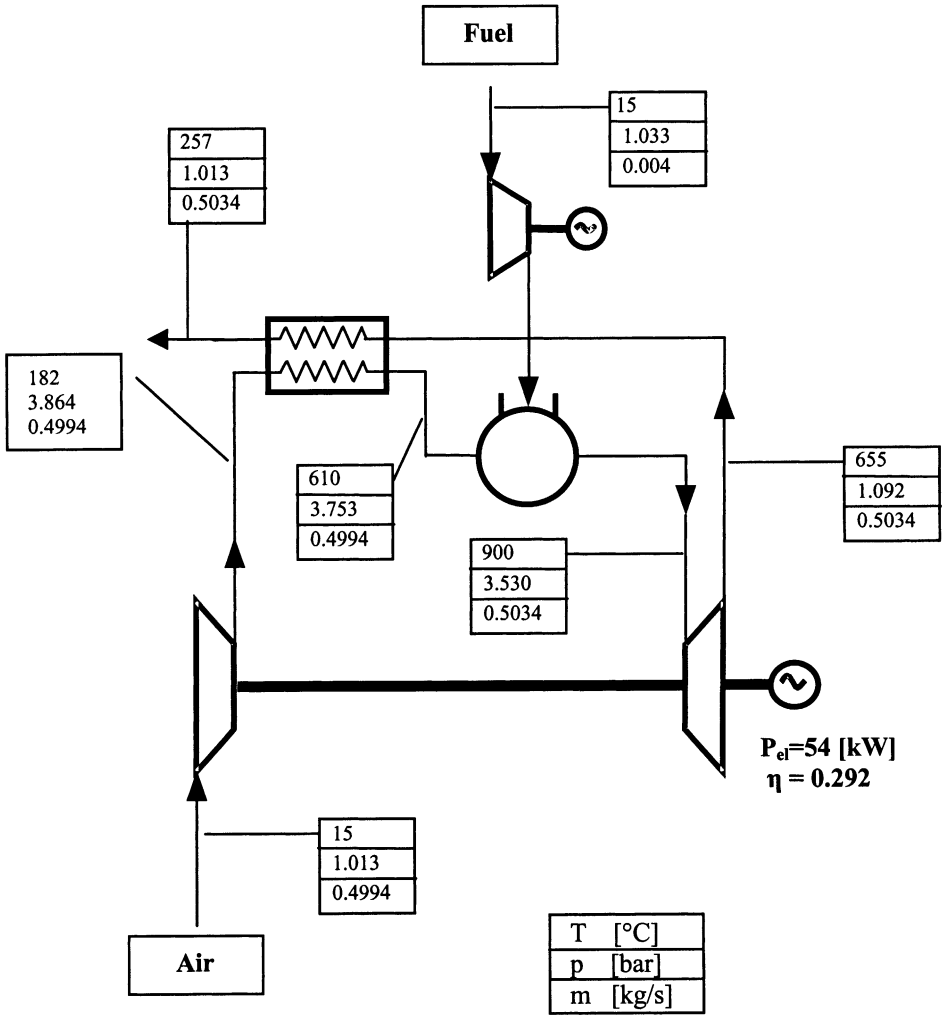

Fig. 2. MGT simplified lay-out.

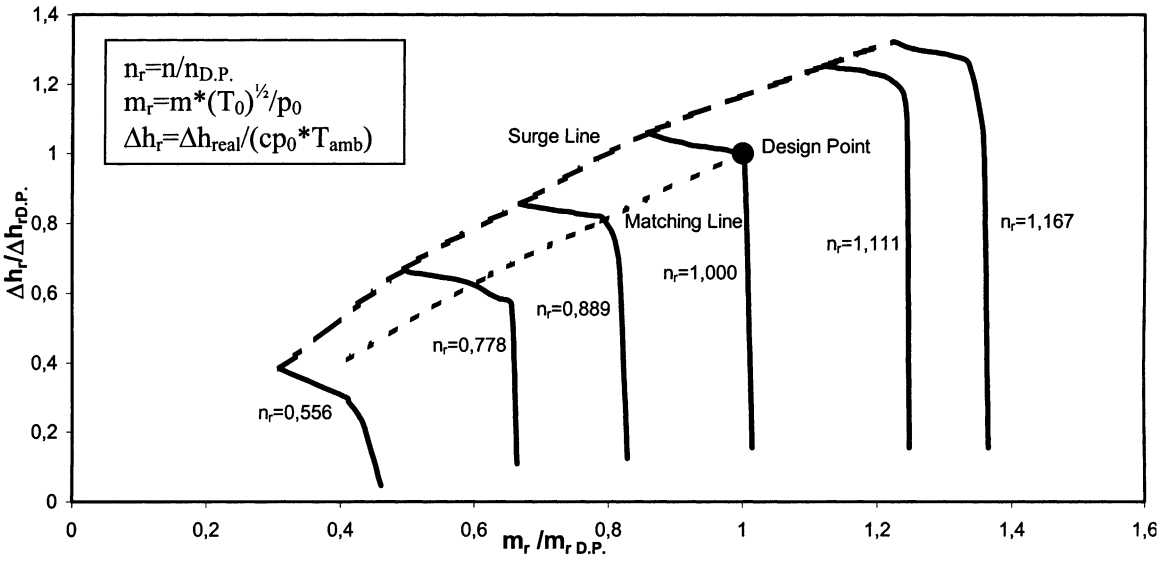

Fig. 3. MGT compressor map.

verify the correct matching of the MGT components; if the matching is not suitable, another pressure ratio value is considered until convergence is reached.

The recuperator module allows the evaluation of temperature distribution at design and off-design operating conditions to be obtained on both the cold and hot sides. At partial load, the heat transfer surface being fixed, an apt correlation [32] is used to evaluate the heat transfer coefficient based on the value of the Reynolds number. The pressure losses at partial load are evaluated as a function of the density and mass flow rate.

Finally, simplified models have been considered for the natural gas compressor (necessary to increase the fuel pressure up to the combustion chamber pressure) and the electrical generator.

The overall model has been positively tested with gas turbine data available in open literature [34]. For example, the matching line for the MGT analysed here is shown in Fig. 3 (where the surge margin is also evident), while the data at the design point are reported in Fig. 2. It is worth noting that the MGT efficiency is about 30% for 54 kW_e electrical power.

2.3. Hybrid system

Fig. 5 shows the simplified layout of the hybrid system, which has been obtained by substituting the SOFC group to the combustor of the MGT plant reported in Fig. 2. The plant design and the size of all the components have been chosen on the basis of indications from the literature on combined

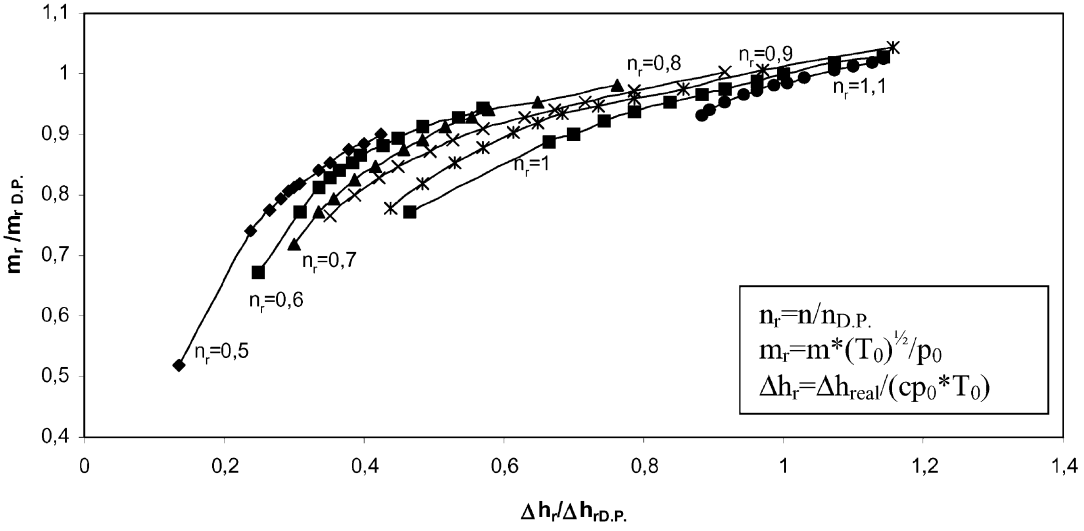

Fig. 4. MGT expander map.

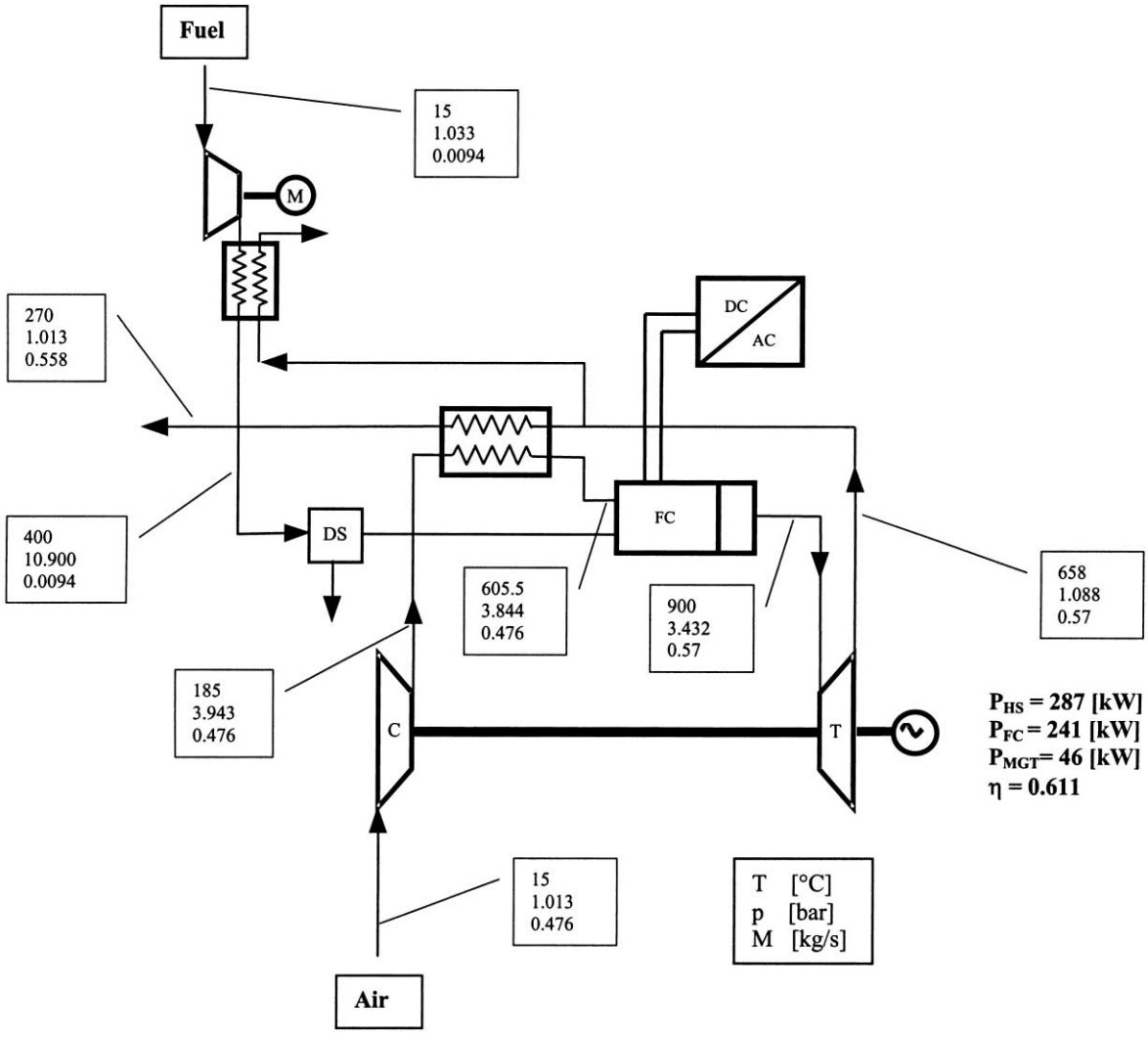

Fig. 5. Simplified lay-out of the hybrid plant (MGT and SOFC), with data at the design-point.

SOFC/MGT plants [11,14]; the MGT has a size of about 50 kW_e, and the SOFC stack has an overall active area of 95 m^2, which produces about 240 kW of power at the design point (the cell specific power is about 2.5 kW/m^2). The simulation model of the hybrid plant has been obtained using a combination of the previously described models of MGT and SOFC groups. The resulting simulation package runs on a personal computer (PIII, 500 MHz, 64 MB RAM) and requires about 15 min for a design point analysis.

3. Results and discussion

3.1. Design performance of the HS

In our case study, the design point of the HS plant is the operating condition where the turbine flow rate, rotational speed, pressure, and turbine inlet temperature are compatible with the limitations of this technology and the size of the turbine under consideration. When the MGT has been defined, the SOFC group is designed to be fed with the same air flow rate, operated at the MGT pressure, and have an exhaust temperature equal to the turbine inlet temperature (TIT) of the MGT. Actually, there are other ways of selecting the design point; for example, starting with the data of an existing SOFC system and finding the apt MGT (if it exists). This subject is very important and will be addressed in a future work which will include an optimisation approach.

Even if the best operating condition for the combined plant is slightly different from the design point chosen on the basis of the previous procedure, the main goal of this work is the study of the behaviour of a hybrid system under off-design conditions, which could only be marginally affected by the choice of the design point. In our case study, the typical operating conditions were as follows: pressure 3.8 bar; fuel (methane) flow rate and inlet temperature 0.094 kg/s and 15°C, respectively; oxidant (air) flow rate and inlet temperature 0.47 kg/s and 15°C, respectively. The design point temperature, pressure and flow rate values of each module of the plant are shown in Fig. 5. It is interesting

to note that the HS efficiency is higher than 60%, which is particularly important considering the small size (287 kW_e) of the whole plant. This efficiency is higher than that of advanced large combined cycle (>200 MW) plants using steam as the blade cooling medium. It is also important to observe that at design condition the MGT power is about 16% of the whole HS power, while the ratio between MGT and SOFC power is 19%. However, the design point performance is not sufficient to determine if the HS is a good system for the distributed electricity market and cogeneration applications, as an HS is expected to operate also at part-load conditions during its operating life.

3.2. Off-design performance of the SOFC group

In order to facilitate the understanding of the results of the overall plant simulation, the performance characteristics of the SOFC group alone (i.e. not inserted in the HS) are presented and discussed. In particular, the current–voltage curves obtained under different operating conditions for the overall SOFC group (i.e. including the fuel cell stack, the mixer and the reformer) are presented. It is important to note that the influence of the reformer on the overall performance is not very significant, and the behaviour of the group is dominated by the characteristics of the SOFC reactor. In all the runs, the operating conditions have been kept as close as possible to those applied to the HS, in order to analyse the behaviour of the SOFC group close to the plant design point and under typical off-design conditions for the HS. For example, one of the most important parameters influencing the SOFC performance is the operating temperature of the fuel cell stack; for this purpose, and in order to vary only one parameter at a time, some runs were made where the operating temperature was not free to vary according to the energy balance (Eq. (23)), but it was imposed as input datum, in order to determine its effects on the electrical performance. Those results are interesting also for a better understanding of the plant behaviour (Section 3.3). In all the runs, the pressure was 3.8 bar, the utilisation factors were kept constant at 0.85 and 0.26 for methane and oxygen, respectively (where the methane utilisation factor is defined as $U_{CH_4} = F_{H_2,consumed}/4F_{CH_4}$) and the inlet temperatures of the gases were 400 and 607°C at the fuel and air sides, respectively; all these values are very similar to those at the design point (Fig. 5 and Section 3.1). Fig. 6 shows the current–voltage simulated characteristic curves at different stack operating temperatures, from 850 to 1000°C. The curves show typical SOFC straight lines [19]; by decreasing the temperature, the slope of the lines increases exponentially, due to the exponential increase of both the activation and ohmic resistances, as shown in Fig. 7. The latter figure also shows the relative importance of the different resistance terms: ohmic and activation polarisations are almost of the same magnitude, while contact resistances are about one third of the previous effects, in agreement with data previously reported in the literature [27].

The efficiency of the SOFC module is an important parameter to be studied to understand plant behaviour under part-load conditions. In Fig. 6, the straight lines which represent the current–voltage curves, also represent the efficiency of the SOFC module; the direct ratio between voltage and efficiency is due to the fact that the fuel utilisation is kept constant along all the curves.

The power is a parabolic function of the cell current density (Fig. 8), and thus the plot of the efficiency as a function of power has the behaviour shown in Fig. 9: this is the 'off-design map' of the SOFC module (operating at imposed temperature), which has an interesting feature. In fact, if we take into consideration a fixed temperature for the SOFC stack, for each value of the power supplied there are

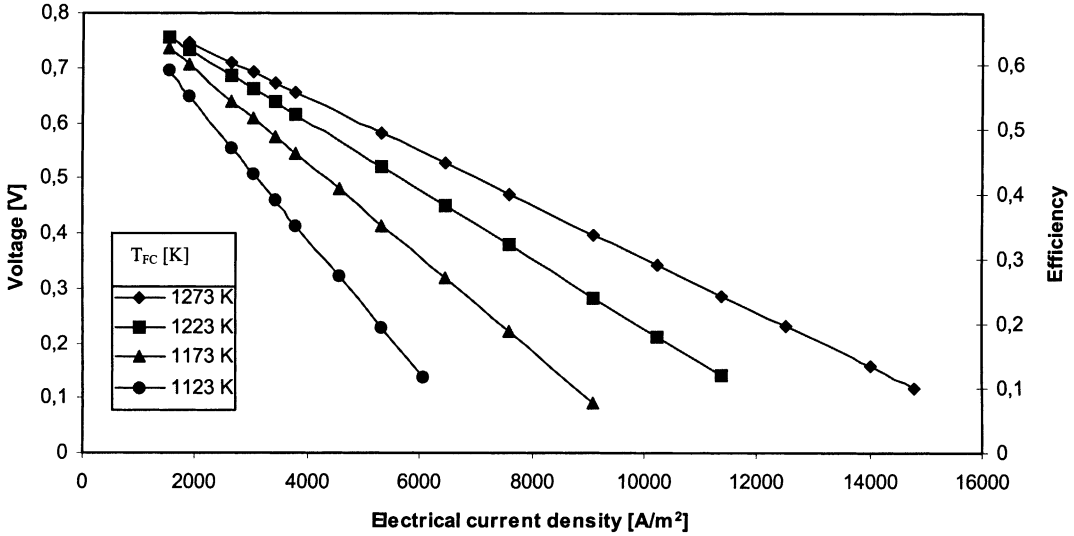

Fig. 6. SOFC group voltage and efficiency vs. electrical current density, at fixed fuel cell operating temperature, and $U_f = 0.85$ and $U_o = 0.26$. Variable parameter: fuel cell temperature.

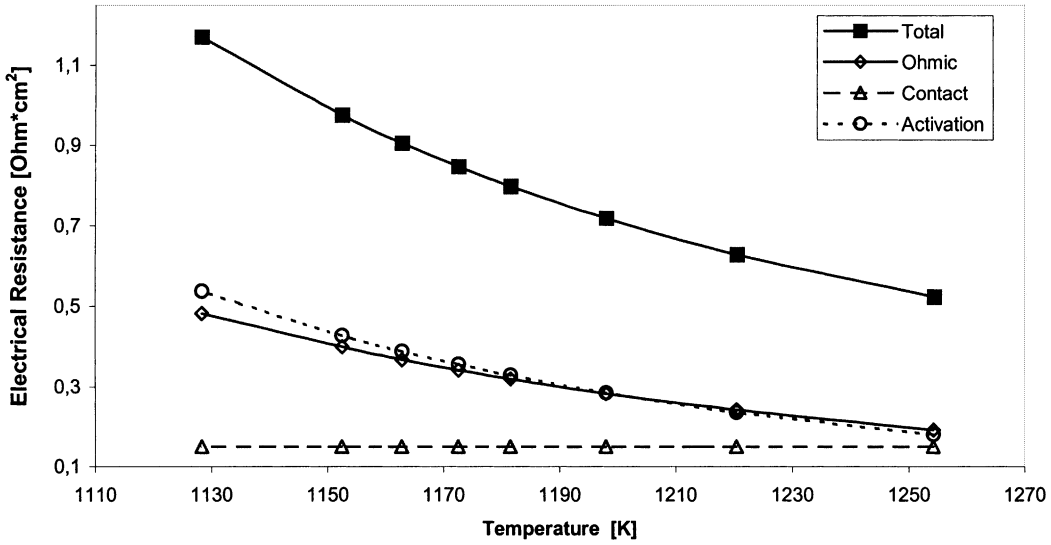

Fig. 7. SOFC group electrical resistance vs. fuel cell temperature, with $U_f = 0.85$, $U_o = 0.26$.

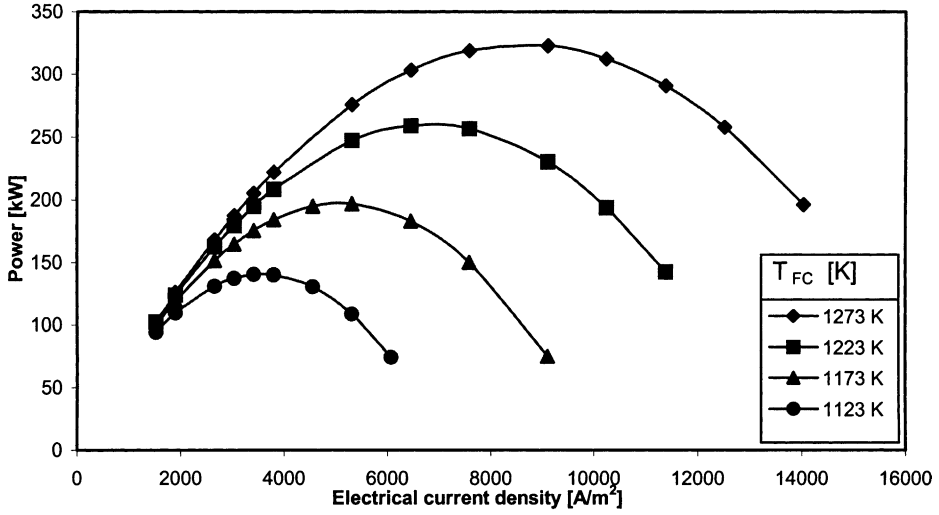

Fig. 8. SOFC group power vs. electrical current density at fixed fuel cell operating temperature, and $U_f = 0.85$ and $U_o = 0.26$. Variable parameter: fuel cell temperature.

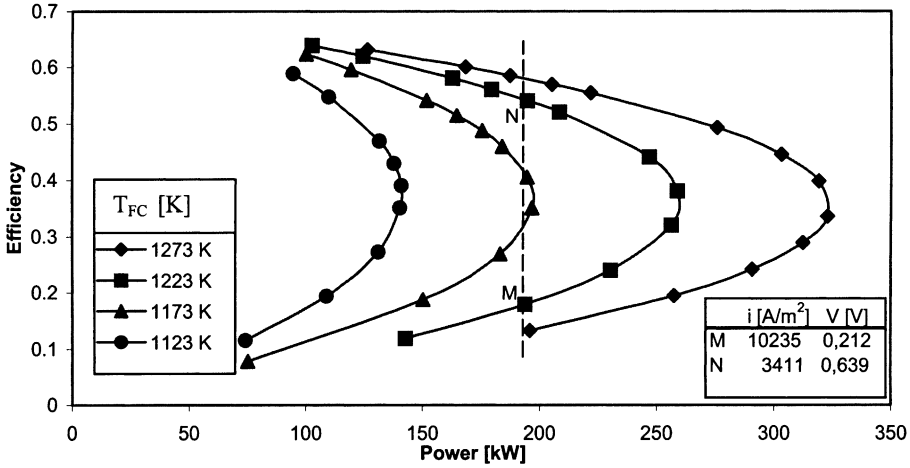

Fig. 9. SOFC group efficiency vs. power at fixed fuel cell operating temperature, and $U_f = 0.85$ and $U_o = 0.26$. Variable parameter: fuel cell temperature.

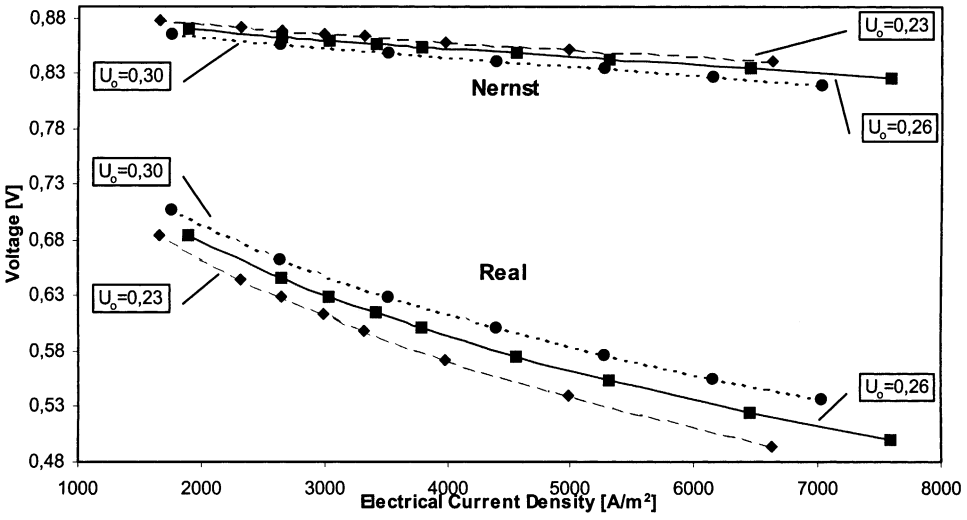

Fig. 10. SOFC group voltage vs. electrical current density, calculated with $U_f = 0.85$. Fuel cell temperature evaluated according to the energy balance. Variable parameter: U_o.

two alternative modes of operation (M and N): in both points the operating parameters of temperature and fuel and oxygen utilisation have the same value and the electrical current density and the efficiency differ; the points at high efficiency correspond to low electrical current densities, and the points at low efficiency correspond to high electrical current densities. The features of these maps will be further discussed with reference to the overall plant performance.

In addition to the study of the behaviour of the SOFC under isothermal conditions, some more runs were carried out in adiabatic conditions (i.e. the operating condition of the SOFC group in the HS). In this case, the complete simulation model was used, including the thermal balance of the SOFC reactor; thus, the operating temperature of the stack was not constant, and it was evaluated on the basis of the energy balance (Eq. (23)). Again, in all the runs the utilisation factors were kept as 0.85 and 0.26 for methane and oxygen, respectively; the inlet temperatures of the gases were kept at 400 and 600°C at the fuel and air sides, respectively. Fig. 10 shows the current–voltage characteristic curves and Fig. 11 shows the variation of temperature along each characteristic curve. As the stack temperature is about 1000°C at a current density of 8000 A/m^2, and the cell temperature increases by increasing the electrical current density, no runs were carried out at a higher current density as the operating temperature would grow beyond the acceptable operating values. The variation of temperature which takes place by increasing the current density (Fig. 11) is due to the increased energy dissipations under these conditions; due to this increase of temperature, the current–voltage

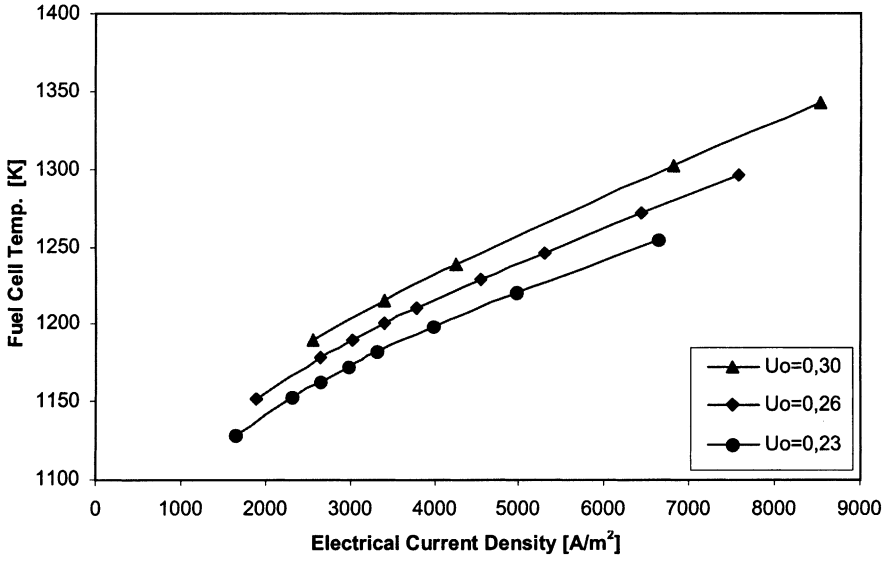

Fig. 11. Fuel cell temperature vs. electrical current density, calculated with $U_f = 0.85$. Fuel cell temperature evaluated according to the energy balance. Variable parameter: U_o.

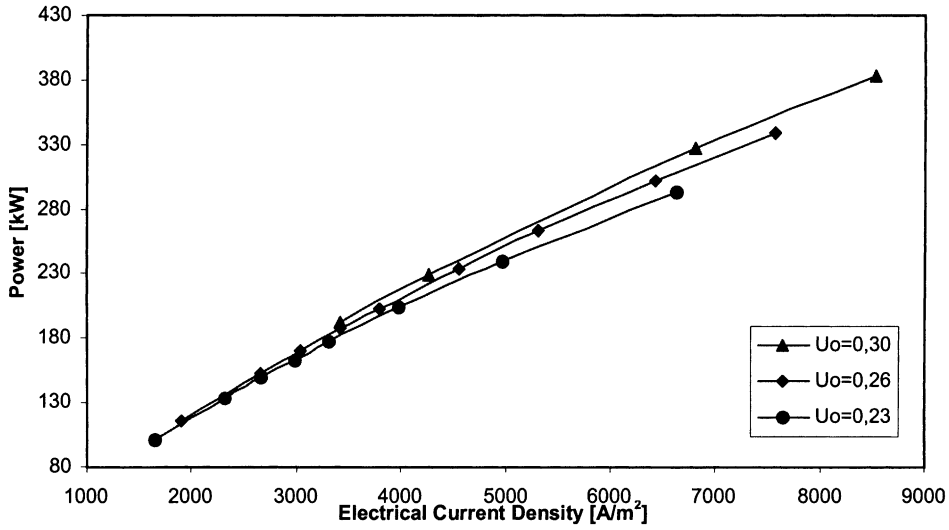

Fig. 12. SOFC group power vs. electrical current density, calculated with $U_f = 0.85$. Fuel cell temperature evaluated according to the energy balance. Variable parameter: U_o.

curves (Fig. 10) are not perfectly straight lines, nor is the Nernst voltage perfectly constant.

Fig. 12 is analogous to Fig. 8, and shows the power of the SOFC group as a function of the electrical current density. In this case, the curves show an increasing trend in the entire operating range under consideration, which is similar to the left branches of the curves reported in Fig. 8. In an analogous way, Fig. 13 shows the efficiency as a function of the power supplied by the SOFC module, and, again, only one branch (i.e. the upper branch) of the analogous curve, shown in Fig. 9, is visible. Figs. 10–14 also show the effect of the oxygen utilisation factor, and in particular Fig. 13 demonstrates that the efficiency versus power curves increase when the oxygen utilisation factor increases. This can be explained by the fact that higher oxygen utilisation factors involve a smaller air flow rate being fed to the fuel cell stack, which causes an increase in temperature and, as a consequence, an exponential decrease of the overpotentials, and finally an increase of the efficiency of the conversion process (it must be mentioned that, when the oxygen utilisation factor increases, the average oxygen molar fraction decreases, with an unfavourable effect on the cathodic polarisation; however, the latter effect is *linear*, and since the previously mentioned effect of temperature is *exponential*, this is prevailing).

3.3. Off-design of the HS at constant turbine rotational speed

When a variable speed control system is not available, the only possible way to vary the power supplied by the plant (part-load operation) in a system including an MGT is to

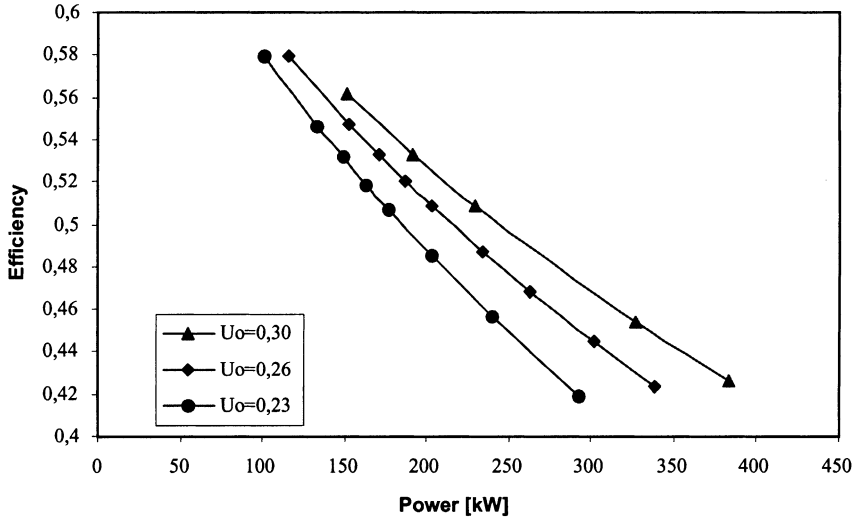

Fig. 13. SOFC group efficiency vs. power, calculated with $U_f = 0.85$. Fuel cell temperature evaluated according to the energy balance. Variable parameter: U_o.

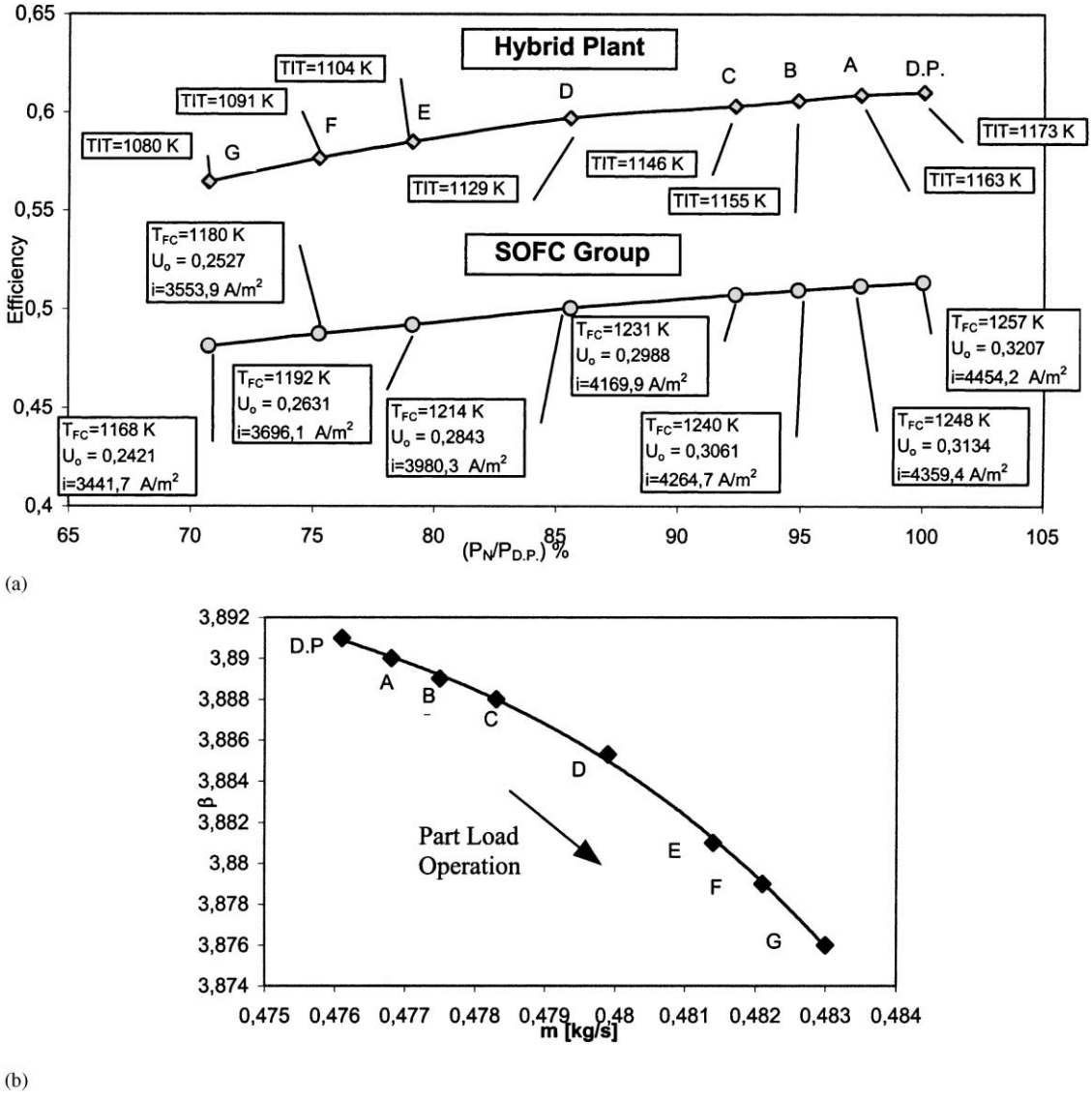

Fig. 14. (a) Hybrid plant and SOFC group efficiencies vs. net non-dimensional plant power at fixed MGT rotational speed (85,000 rpm). T_{FC} (fuel cell temperature), U_o (oxygen utilisation factor), i (current density) and TIT (turbine inlet temperature) are reported at the inset (D.P.: design point; A, B, . . ., G: part-load conditions). (b) Compressor operating line at 85,000 rpm (D.P.: design point; A, B, . . ., G: refer to Fig. 14a).

vary the overall fuel flow rate to be fed to the plant. Some simulations have been made, where the fuel flow rate has been changed by keeping the SOFC fuel utilisation factor constant at 0.85 (and thus different fuel flow rates correspond to proportionally different electrical currents supplied by the SOFC stack). On the other hand, the air flow rate is an independent parameter, which is evaluated on the basis of the matching of the MGT expander, the MGT compressor, and the stack, thus the oxygen utilisation is not constant throughout the simulations.

Fig. 14a shows the response of the overall plant and the SOFC group to a variation of the fuel flow rate (from the design point (DP) to the part load conditions A, B, . . ., G). We would like to point out that a direct comparison between the SOFC and HS efficiencies is not possible, since they are evaluated with slightly different procedures. In fact, the efficiency of the plant is calculated as the ratio between the net power produced and the LHV of the feeding fuel, while the efficiency of the stack is the ratio between the power supplied by the stack alone and the LHV of the fuel supplied to the plant. Thus, the power consumption of the air and fuel compressors and the mechanical losses are not taken into account in the efficiency of the fuel cell group, while they are considered in evaluating the efficiency of the overall plant. To give an idea of the relative importance of all the contributions, at the design point the fuel cell and the MGT expander supply 242 and 136 kW, respectively, the air compressor consumes 82 kW and the methane compressor and mechanical and electric efficiency account for 9 kW overall. Thus, as the compressors serve the SOFC group as well as the turbine, it would be realistic to subtract a part of their power consumption from the power supplied by the

SOFC group in evaluating the SOFC efficiency. In other words, the increase of efficiency due to the presence of the microturbine is not simply the difference between the overall plant and the SOFC group efficiencies (which could erroneously be calculated from Fig. 14a as about 10%). However, it is not a simple matter to determine how to share the power losses between the turbine and the SOFC group, and this matter lies beyond the scope of this work [19].

Fig. 14a shows that when the power supplied by the SOFC group decreases, the efficiency decreases as well. This would appear to contradict what was reported previously in Fig. 13, where, for each value of the air utilisation factor, the efficiency was a decreasing function of the power. However, it must be taken into account that the behaviour of the SOFC group of the plant cannot be simply compared to the behaviour of the SOFC group alone, as considered in Section 3.2. In particular, the curves reported in Fig. 13 were obtained at constant air utilisation factors, and, as already mentioned, that condition does not apply when the SOFC group is integrated in the hybrid plant. The labels reported in Fig. 14a show that the oxygen utilisation factor varies heavily, decreasing from 0.32 to 0.24 when the power percentage changes from 100 to 70%. The reason for the air utilisation factor varying is related to the operating conditions of the MGT compressor. In fact, at constant rotational speed, the variation range of the compressor flow rate is rather narrow (see Fig. 14b), and thus the air flow rate is almost constant, resulting in a sensitive variation to the oxygen utilisation at different current densities. This oxygen utilisation variation is the cause of the stack temperature varying from 984 to 895°C, and thus the efficiency varying from 52 to 48%.

The efficiency versus power curve of the plant is parallel to the efficiency versus power curve of the SOFC group (Fig. 14a), which means that the power supplied by the MGT, minus all the power losses, is directly proportional to the fuel flow rate through all these simulations. The off-design variation of efficiency of the HS is less than 5% under the conditions discussed so far, varying from 61% at the design point to 56.4% at 70% of the nominal power (the minimum part load conditions considered here are determined by the constraints on the MGT expander inlet fluid temperature, about 820°C).

In Fig. 14b, the variation of the MGT operating point is shown for the corresponding A, B, ..., points reported for the HS in Fig. 14a. It is interesting to note that the pressurisation is almost constant, while the air mass flow rate varies by about 1.5%. As a result the required compressor power is practically a constant value. It is also interesting to note that the compressor surge margin increases at part load conditions (points A–G).

3.4. Off-design of the HS at variable turbine rotational speed

The typical operation mode of large size gas turbine plants does not usually involve the possibility of changing the rotational speed of the turbine. The reason for this is that typical plants do not include an inverter, and thus the rotational speed of the turbine is chosen on the basis of the alternate current frequency required by the end user/electrical network. On the contrary, an HS requires the presence of an inverter which converts the electrical current produced by both the fuel cell and the alternator, the latter one being rectified previously, to direct current. Thus, this configuration allows the operation of the turbine at variable rotational speed (variable frequency).

Part-load performance of the hybrid plant at different turbine rotational speeds is depicted in Fig. 15. The results show many interesting features:

1. The overall efficiency of the system is very high, and it agrees well with predictions made by other authors [22–24].
2. All the fixed turbine rotational speed curves show an average decrease of plant efficiency of about 0.05 if the load is reduced by 30%. Only the curves at low turbine rotational speed show a slightly higher loss of efficiency at part load conditions.
3. The possibility of varying the rotational speed of the turbine is of fundamental importance to operate the plant at very high efficiency, even at very low part load conditions. For example, Fig. 15 shows that at a load of about 35% of the nominal operating power, the plant efficiency is about 52% at 65,000 rpm; in addition, it is interesting to see that at 75% of the nominal operating power the efficiency increases from 57.6 to 60–61.7% by decreasing the rotational speed from 85,000 to 80,000–75,000 rpm, respectively. With reference to Fig. 15, we would like to point out here that, for each turbine rotational speed, the overall plant has been simulated between a maximum load obtained when the turbine inlet temperature is maximum (900°C), and a minimum load reached when the turbine inlet temperature is about the minimum operating value (about 820°C).
4. The advantage of the hybrid system compared to a traditional MGT plant is evident from Fig. 15 at both the design point and at part-load conditions.

Again, in order to investigate the performance of the different parts of the plant at part-load conditions in further detail, attention has been restricted to the SOFC group itself. The results are reported in Fig. 16 and show that at each fixed value of the turbine rotational speed the behaviour of the SOFC group is very similar to that previously reported in Fig. 15 for the overall plant. The interesting feature reported in this figure is that the fuel cell efficiency increases by decreasing the turbine rotational speed, while the opposite is true for the overall plant. It is possible to give an explanation for this effect by considering the broken curves in Fig. 16, along which the efficiency increases by decreasing the power. It can be noticed (labels in Fig. 16) that along each

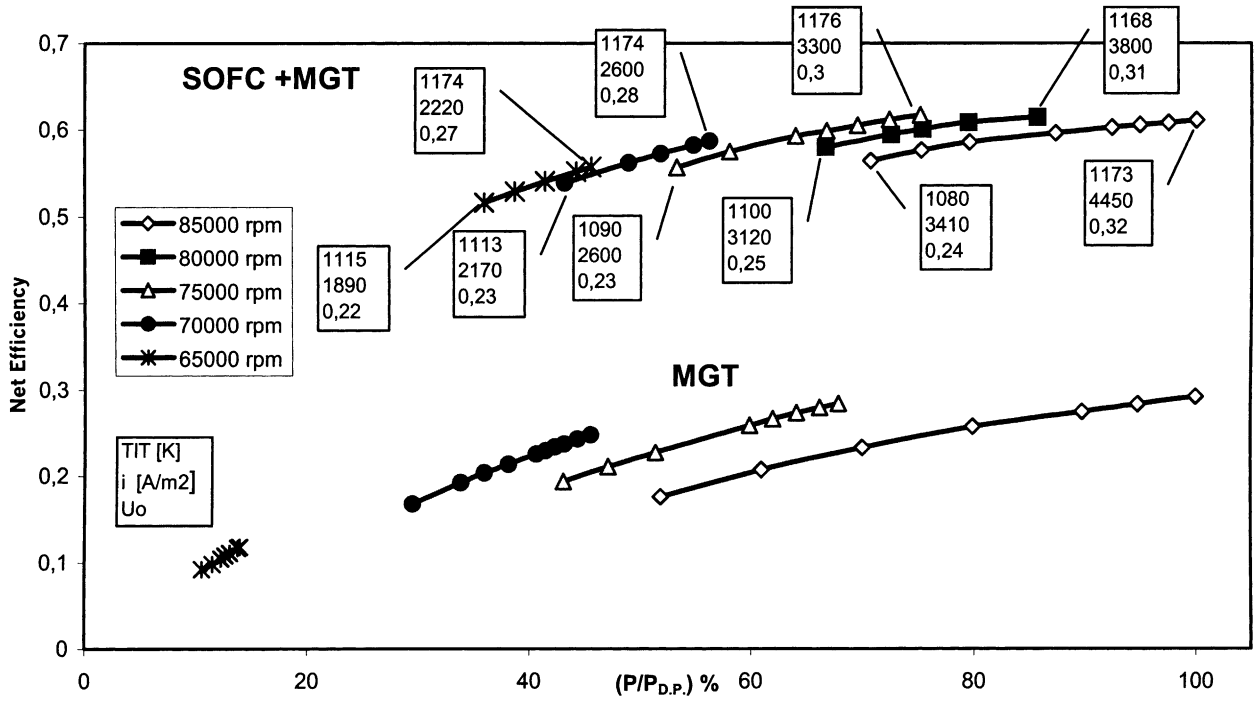

Fig. 15. Hybrid plant and micro gas turbine net efficiencies vs. net non-dimensional power (at MGT variable speed).

broken curve both the temperature and the oxygen utilisation of the fuel cell remain fairly constant; this is due to the fact that, when the SOFC module is integrated into the plant, there is an interesting effect of the recuperator module when the variable speed control system is utilized. In fact (labels in Fig. 16), in this case the load change involves a reduction of the air flow correlated to the speed reduction, while for fixed speed control the load reduction is only due to the fuel mass flow rate variation (corresponding to a small air flow rate reduction, see Fig. 14b). Therefore, under variable speed control conditions, at part load the recuperator effectiveness increases significantly with decreasing air flow, until a very low value is reached (below 10%), where thermal performance is degraded by longitudinal conduction in the heat

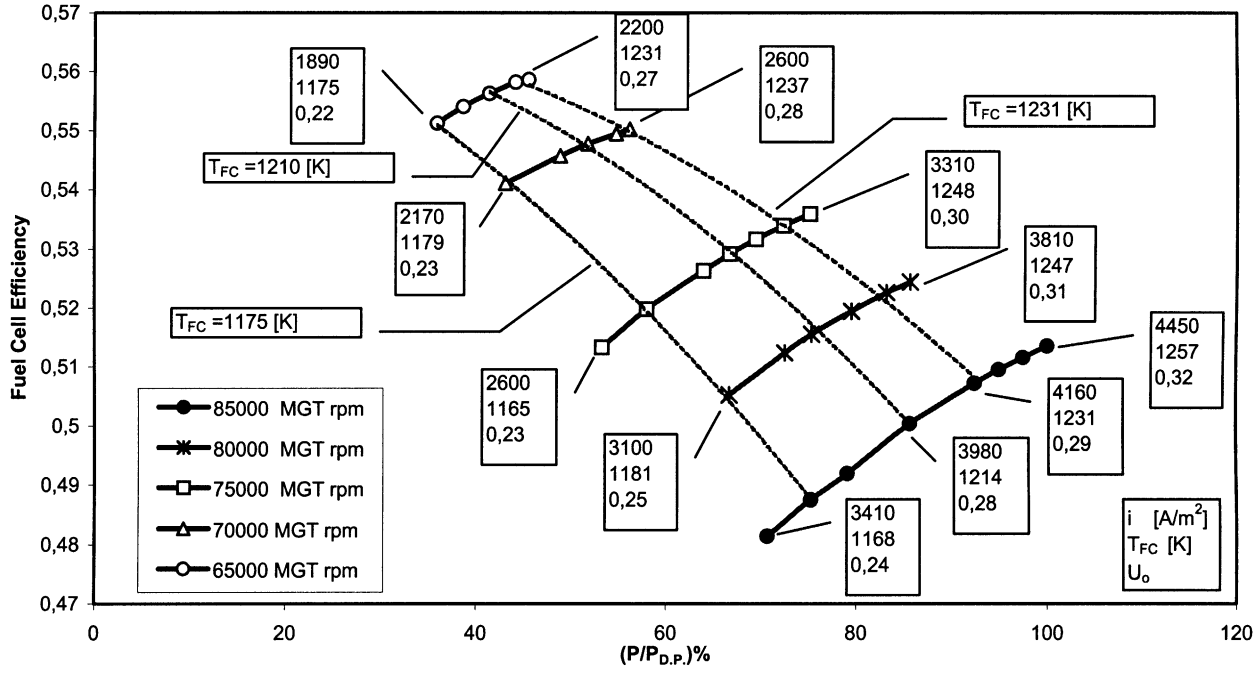

Fig. 16. SOFC group performance at HS part-load when the MGT variable speed system is utilised.

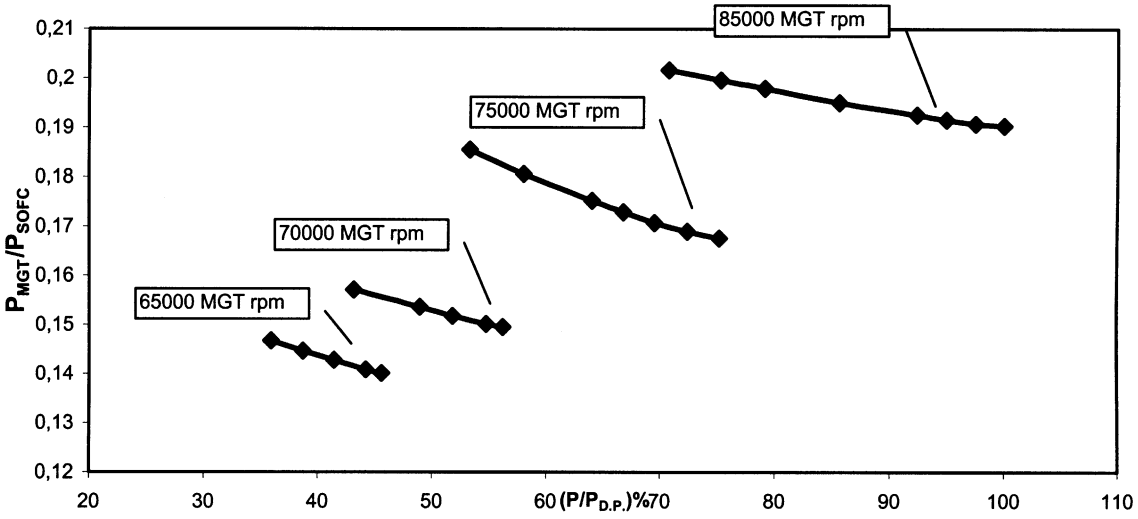

Fig. 17. MGT to SOFC group net power ratio at part load conditions when the MGT variable speed control system is utilised.

exchanger, particularly for matrices of very high compactness [36]. This behaviour of the recuperator effectiveness allows the air temperature at the inlet of the stack (recuperator outlet) to increase at part load, and therefore the SOFC temperature remains fairly constant along the broken lines of Fig. 16. Since both temperature and oxygen utilisation factors remain constant along those curves, they coincide with the upper part of the curves in Fig. 9, and this explains the reason why they show an increase of fuel cell efficiency by decreasing the power. It is extremely important that the off-design curves of the SOFC group of the plant lies on the upper, and not on the lower part of the curves reported in Fig. 9. The latter scenario could very well occur for different geometrical or operating parameters for the HS (for example, a smaller SOFC stack), and in that case the off-design curves of the SOFC group (and, as a consequence, of the plant) could show a completely different and unfavourable trend.

The fact that in spite of the increased performance of the SOFC group under part-load conditions, the overall plant shows a decreased performance under the same conditions (Fig. 15) is due to the fact that the efficiency of the fuel cell group alone does not take the power required by the compressor and the off-design of the electrical part of the plant into account, as already mentioned. These effects, and also all the effects related to the off-design of the MGT group, the alternator (efficiency of 85% at 25% load) and the mechanical parts, explain the difference between Figs. 15 and 16.

Finally, it is interesting to analyse the MGT and SOFC power ratio. Fig. 17 shows the P_{MGT}/P_{SOFC} ratio for four different MGT rotational speeds. At high speed (near design point), when the load is reduced the power ratio increases, so the importance of the MGT at part load increases too. This is due to two facts:

1. The MGT practically operates at a fixed point (see Fig. 14b), and its power is almost constant.
2. The SOFC power decreases at part load and fixed rotational speed, as shown in Fig. 16.

When the MGT rotational speed is very low this aspect is more evident.

4. Conclusions

In this paper, the design and off-design performance of a hybrid system (HS) based on the coupling of a recuperated micro gas turbine (MGT) with a high temperature solid oxide fuel cell (SOFC) reactor has been presented and discussed. The MGT, SOFC reactor and HS models have been presented and discussed in depth. The coupling of an MGT (about 50 kW_e) with an SOFC reactor (about 250 kW_e) has shown a potential for an efficiency of over 60% at design point and always over 50% at part load conditions. The different behaviour of the SOFC reactor at off-design conditions has been presented for two cases: when the SOFC reactor temperature is fixed and when this temperature is evaluated on the basis of the complete reactor heat transfer analysis. In the first case the cell efficiency versus cell power (Fig. 8) and the cell power versus current density (Fig. 7) show a parabolic behaviour; in the second case (more similar to the reactor operative conditions in the HS at constant turbine rotational speed), the corresponding curves are different (Figs. 12 and 13) due to the strong influence of the cell temperature on the electrical resistance, the air utilisation factor, etc.

The HS off-design performance has been analysed for two different MGT rotational speed control systems: (1) fixed and (2) variable. At fixed rotational speed the HS performance is very interesting, limited only by the minimum TIT and SOFC temperature values considered here. However, the MGT always operates near its design point (Fig. 14b), and at part load the compressor surge margin increases. In this case

the off-design efficiency of the HS from 61% at the design point to 56.4% at 70% of the nominal power (Fig. 14a). At variable MGT rotational speed it is possible to obtain very high efficiency also at very low part load conditions (Fig. 16). The efficiency is always higher than 50%, also at 30% of the power at the design point. The fuel cell performance in the HS is mainly dominated by the fuel and air flow rates, i.e. the air utilisation coefficient (U_f is considered constant). The importance of the cell operative temperature is also evident.

The power ratio between MGT and SOFC reactors is about 20% at the HS design point, and it increases at part load, using fixed rotational speed. When the variable rotational speed control is used the power ratio decreases from 20 to 15%.

The HS studied here has not been optimised from the design condition performance point of view. In fact two different possibilities are evident:

1. Starting with an existing MGT and choosing the SOFC reactor data, as is done in this work.
2. Starting with SOFC reactor data and choosing the MGT characteristics.

For both these cases an optimum design procedure can be developed, using the model presented here.

Acknowledgements

This study was financially supported by MURST of Italy (Cofinanziamento 1999).

References

[1] J.H. Hirschenhofer, D.B. Stauffer, R.R. Engleman, M.G. Klett, 1998, Fuel Cell Handbook, DOE report DOE/FETC-99/1076, US Department of Energy, Morgantown (WV).
[2] R.H. Wolk, IEEE Spectrum 36 (1999) 45.
[3] T. Ishii, Y Tajima, J. Electrochem. Soc. 142 (1995) 1519.
[4] R. Ihringer, J. Van Herle, A.J. McEvoy, in: Proceedings of the 3rd European SOFC Forum, Nantes (F), June 1998, p. 407.
[5] N. Wu, X. Chen, L. Smith, A. Ignatiev, Abstracts of the 197th ECS Meeting, Toronto (CA), May 2000, Abstract no. 65.
[6] S. de Souza, S.J. Visco, L.C. de Jonghe, Solid State Ionics 98 (1997) 57.
[7] T. Tsai, E. Perry, S. Barnett, J. Electrochem. Soc. 144 (1997) L130.
[8] S. Sunde, J. Electrochem. Soc. 143 (1996) 1930.
[9] P. Costamagna, P. Costa, V. Antonucci, Electrochim. Acta 43 (1998) 375.
[10] W. Drenckhahn, J. Eur. Ceram. Soc. 19 (1999) 861.
[11] W.J. Dollard, J. Power Sources 37 (1992) 133.
[12] R. Diethelm, M. Schmidt, B. Doggwiler, Th. Gamper, M. Keller, K. Honegger, E. Batawi, in: Proceedings of the 3rd European SOFC Forum, Nantes (F), June 1998, p. 87.
[13] R.A. George, J. Power Sources 86 (1999) 134.
[14] S.E. Veyo, C.A. Forbes, in: Proceedings of the 3rd European SOFC Forum, Nantes (F), June 1998, p. 79.
[15] A.F. Massardo, C.F. Mc Donald, T. Korakianitis, ASME Paper 2000-GT-175, and ASME Transactions, in press.
[16] C.F. Mc Donald, ASME Paper 2000-GT-0167.
[17] C. Rodgers, ASME Paper 2000-GT-0626.
[18] V. de Biasi, Gas Turbine World 20 (1999) 12.
[19] S.E. Veyo, L.A. Shockling, J.T. Dederer, J.E. Gillett, W.L. Lundberg, ASME Paper 2000-GT-0550.
[20] F. Massardo, F. Lubelli, J. Eng. Gas Turbines Power 122 (2000) 27.
[21] J. Palsson, A. Selimovich, L. Sjunnesson, J. Power Sources 86 (1999) 442.
[22] K. Hassmann, W.K. Heidug, S. Veyo, Brennstoff Wärme Kraft 11/12 (1999) 40.
[23] S. Campanari, J. Eng. Gas Turbines Power 122 (2000) 239.
[24] S. Campanari, E. Macchi, ASME Paper 99-GT-84.
[25] S. Campanari, Power plants based on solid oxide fuel cells combined with gas turbine cycles, Ph.D. Thesis, Politecnico di Milano, 1998 (in Italian).
[26] P. Costamagna, E. Arato, P.L. Antonucci, V. Antonucci, Chem. Eng. Sci. 51 (1996) 3013.
[27] P. Costamagna, K. Honegger, J. Electrochem. Soc. 145 (1998) 3995.
[28] P. Costamagna, J. Power Sources 69 (1997) 1.
[29] N.F. Bessette II, W.J. Wepfer, J. Winnick, J. Electrochem. Soc. 142 (1995) 3792.
[30] E. Achenbach, J. Power Sources 49 (1994) 333.
[31] U. Bossel, Facts and figures, IEA Task Report, Berne, April 1992.
[32] L. Magistri, Gas microturbines and solid oxide fuel cells for the distributed generation of electrical power, Master's Thesis, University of Genoa, 1999 (in Italian).
[33] H. Uchida, M. Shiraki, A. Bessho, Y. Yagi, ASME Paper 94-GT-73.
[34] P. Pilidis, Digital simulation of gas turbine performance, Ph.D. Thesis, University of Glasgow, USA, 1983.
[35] K.R. Pullen, N.C. Baines, S.H. Hill, ASME Paper 92-GT-93.
[36] C.F. Mc Donald, ASME Paper 75-GT-50.